Green Chemistry

PAPER

View Article Online
View Journal | View Issue

Cite this: *Green Chem.*, 2026, **28**, 242

Green and efficient cell wall nano-reconstruction under ambient temperature towards strong cellulosic aerogels

Xiaoying Xu, [a] Arezu Sehati, [a] Lukas Marcos Celada,[b] Peter Olsén,[b] Lars Berglund [a] and Yuanyuan Li *[a]

Cellulosic aerogels show great promise for diverse applications. However, their widespread adoption is hindered by energy-intensive processing and limited mechanical properties. This work presents a green and efficient approach for strong cellulosic aerogel synthesis through cell wall nano-reconstruction using one-step NaOH (10 wt%) treatment of wood at ambient temperature. The obtained cellulosic aerogel (wood aerogel) showed partially preserved hierarchical structure and nanofibril networks filled lumen, leading to a combination of high specific surface area (202 m^2 g^{-1}) and a high yield strength (4.3 MPa). The generation of mesoporosity and the building of nanofibril networks were studied in detail. NaOH provided cell wall swelling and partial extraction of deacetylated xylan, generating nanoporosity in the cell wall. The extracted xylan then aggregated and rearranged into nanofibril networks occupying the lumen. The technology developed for wood aerogel synthesis and the understanding of wood aerogel formation pave the way for green cell wall nanoengineering towards advanced materials design.

Received 22nd July 2025,
Accepted 6th October 2025

DOI: 10.1039/d5gc03785a

rsc.li/greenchem

Green foundation

1. Top-down cell wall engineering was applied to fabricate cellulosic aerogels with exceptional combined properties (specific surface area of 202 m^2 g^{-1} and compressive strength 4.3 MPa). This method significantly reduces energy and chemical consumption by bypassing the intensive nanocellulose extraction required in conventional bottom-up approaches, while yielding aerogels (wood aerogels) with superior performance to nanocellulose-based counterparts.
2. Ambient temperature NaOH treatment eliminates the need for toxic chemicals, expensive solvents, and energy-intensive processes typically employed in aerogel production. A detailed investigation of the structural evolution and formation mechanism revealed how cell wall reconstruction creates the unique mesoporous structure of wood aerogels.
3. This green nanoengineering strategy paves the way for strong, scalable, bio-based aerogel production, offering a sustainable alternative to petroleum-based foams in thermal insulation, adsorption, and catalytic applications.

Introduction

Cellulosic aerogels are generally mesoporous (2–50 nm) solid networks with high porosity (>90%), and high specific surface area (SSA, 100–600 m^2 g^{-1}).[1] Cellulosic aerogels are attractive in diverse applications such as thermal superinsulation,[2] adsorption/separation,[3,4] tissue engineering,[5] *etc*. Their sustainable origin offers additional advantages in material development. However, the fabrication of cellulosic aerogels is usually energy-intensive and time-consuming. Low mechanical performance (compression yield strength normally <1 MPa) is also a restriction.

Top-down fabrication of cellulosic aerogels offers a promising solution. Wood aerogel, a cellulosic aerogel processed directly from natural wood, has been proposed.[6] Wood aerogels are anisotropic and mesoporous with microfibril networks occupying the originally empty lumen, see Fig. 1. The formation of mesopores and partial preservation of natural cell wall structure enable wood aerogels with a unique combination of high SSA (>180 m^2 g^{-1}), mechanical strength (>1.2 MPa), and directional conduction channels.[6] The collection of intriguing properties makes wood aerogels promising for various applications, such as thermal insulation,[7,8] wastewater treatment[9,10] and hydrovoltaic energy harvesting.[11,12] In the literature, delignified wood followed by hemicellulose removal is described as wood aerogels as well,[9,13–17] where macropores (*e.g.*, lumen with diameter >10 μm) count for the majority. In

[a]*Wallenberg Wood Science Center, Department of Fiber and Polymer Technology, KTH Royal Institute of Technology, SE-10044 Stockholm, Sweden.*
E-mail: yua@kth.se
[b]*Laboratory of Organic Electronics (LOE), Department of Science and Technology, Linköping University, SE-60174 Norrköping, Sweden*

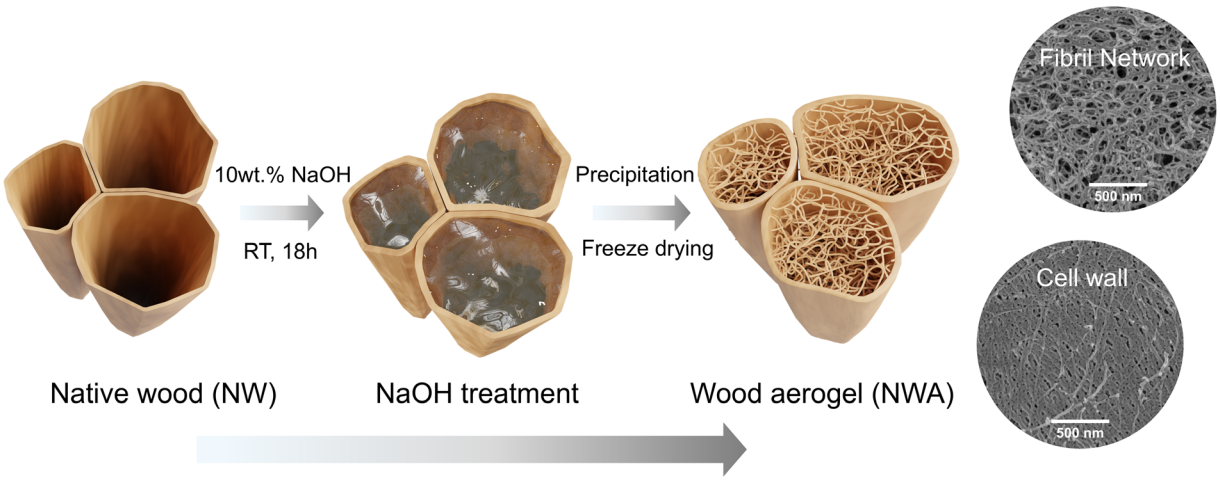

Fig. 1 Schematic illustration of wood aerogel preparation. From cell wall swelling to the building of microfibril networks in lumen were shown. SEM images on the right display the fibril networks and porous cell wall of NWA.

this work, wood aerogels only refer to structures with mainly mesopores (2–50 nm).

Despite recent progress, wood aerogel fabrication still requires substantial chemical input and energy consumption. Wood aerogel synthesis can be generally assigned into two categories: additional polymer filling and reassembly of cell wall components. The former is a straightforward strategy to decrease macropores (*e.g.*, lumen) and increase mesoporosity in the lumen. Monomers were infiltrated into wood templates, followed by *in situ* polymerization. Cross-linked polymers form porous networks in the lumina, while the cellular structure of wood remains intact. Composite aerogels could be achieved upon proper drying of the composite hydrogel. Polyacrylamide (PAM),[18] poly(vinyl alcohol) (PVA),[19,20] poly(acrylic acid) (PAA),[19–21] and poly(*N*-isopropylacrylamide) (PNIPAM)[22] were infiltrated into wood targeting strong, functional wood hydrogels. Fibril networks were revealed from their scanning electron microscopy (SEM) images. Gelatin-infiltrated wood shows a porous honeycomb structure with tunable porosity.[23] Although lumina could be filled with porous polymers, infiltration is time-consuming, and monomers are usually petroleum-based. In comparison, reassembly of cell wall components is more advantageous in wood aerogel synthesis, where biopolymers in wood are utilized without introducing extra polymers. One reported mechanism is the partial dissolution and regeneration of cell wall constituents, primarily cellulose. Upon chemical treatment, dissolved cell wall substances diffuse to the lumen and are confined in cells. With the addition of anti-solvents, solubilized biopolymers are phase-separated from the solvent and form fibril networks in the lumen. Wood aerogel synthesized by lithium chloride in *N*,*N*-dimethylacetamide (DMAc/LiCl) is a pioneer work under this circumstance.[6] A guanidinium phosphorus-based ionic liquid ([MTBD][MMP]) was then explored to better control the formation of nanocellulosic networks by tailoring the cell wall dissolution and mass diffusion.[7,24] However, these chemicals raise concerns over high cost, moisture-sensitivity, and sustainability. In pursuit of eco-friendly, sustainable production, an alteration to greener chemicals is required. NaOH treatment attracts lots of attention because it is scalable, cost-effective, and easy to recycle.[25] NaOH enables cellulose dissolution at 7–10 wt% concentration and below 0 °C.[26,27] Both NaOH–water (8 wt%, −6 °C)[11] and NaOH–urea–water (7 wt%, −13 °C)[12] could achieve wood aerogels with high porosity and large SSA. However, processing under sub-zero temperatures is energy-intensive.[28]

Partial dissolution and regeneration play a key role in wood aerogel synthesis, where dissolution helps migrate cell wall polymers into the lumen. Most literature targeted cellulose dissolution and regeneration,[6,7] while dissolving cellulose is inherently challenging. Nevertheless, is cellulose dissolution a prerequisite for the reassembly of cell wall components? Wood cell walls can be considered as cellulose microfibril bundles embedded in the matrix of hemicellulose and lignin.[29] This structural arrangement limits the accessibility of cellulose, hindering dissolution as reported in the previous studies.[6,7] In addition, cellulose dissolution was reported to require more time due to its high crystallinity.[30] Hemicellulose is another major cell wall polymer, comprising 20–35% of dry wood mass.[29] Hemicellulose is amorphous with a low degree of polymerization (DP, 80–200) and exhibits higher accessibility than cellulose.[31] Extracting and confining hemicellulose within the lumen could be an alternative approach for preparing wood aerogels. NaOH is particularly suitable for this purpose, as it can efficiently extract hemicellulose[32–34] and swell cellulose fibers[35,36] at room temperature.

This work aims to develop a facile, green approach for wood aerogel synthesis *via* one-step ambient temperature NaOH treatment, as shown in Fig. 1. Instead of targeting cellulose dissolution, hemicellulose extraction was employed to achieve both high SSA and mechanical strength of wood aerogels. Hemicellulose detached from the cell wall, confined and rearranged into networks occupying the lumen. Compared with reported approaches, ambient temperature NaOH treat-

ment is greener and more efficient. Moreover, the formation of wood aerogel structure is proposed, which could help understand and control cell wall engineering techniques.

Results and discussion

To evaluate the feasibility of forming wood aerogels under green ambient temperature, native balsa wood (NW) was treated with 10 wt% NaOH at room temperature for 3 h to 24 h. NaOH concentration determines the size of hydrated ions,[27] the extractability for hemicellulose,[32–34] and the final cellulose type.[35,36] 10 wt% was chosen here because it resulted in a significant structure change while preserving the cellulose crystal type of NW. NW has a light brown appearance, thin cell walls, and large empty lumen space, as shown in Fig. 2a. After 3 h treatment, some entangled fibrils formed in the lumen (Fig. 2b). With increasing treatment time, a larger amount of fibril networks were generated (Fig. 2c–f), forming a wood aerogel (NWA) directly utilizing the natural wood structure. Chemical composition of samples during the treatment was also monitored, as shown in Fig. 2g. Hemicellulose content drops with extended treatment time. Hemicellulose is a group of mostly amorphous cell wall polysaccharides, which can be solubilized (and degraded) by alkali. Nevertheless, the hemicellulose extractability by NaOH is restricted in this case, due to NaOH concentration and operating temperature, as well as the presence of lignin[37] in native wood. Lignin content decreased once treated with NaOH. Weight losses of samples were measured (Fig. S1) with values varying from 14% to 23%, as the treatment time increased from 3 h to 24 h. SSA of wood samples essentially increased as the treatment time changed from 3 h (148 m^2 g^{-1}) to 18 h (202 m^2 g^{-1}), as shown in Fig. 2h. However, longer treatment time does not further increase SSA, probably because of the shrinkage caused by alkali (Fig. S1). Fig. 2i displays the corresponding pore size distribution. Short NaOH treatment time, such as 3 h and 6 h, mostly generate small pores around 3–5 nm and a small portion of pores from 20–40 nm. Longer treatment time (>12 h) gives aerogels with broader pore size distribution, predominantly between 3–10 nm. NWA from 18 h treatment possesses the highest SSA and is selected for further analysis.

Fig. 3a displays the appearance of NWA, which has a lighter color and some volume shrinkage (20%) compared with NW. The morphology of wood aerogels on the microscale was investigated in detail. Almost all empty lumen space was occupied by entangled fibril networks, which can be observed from both transverse and tangential planes, as shown in Fig. 3a–c. Gaps

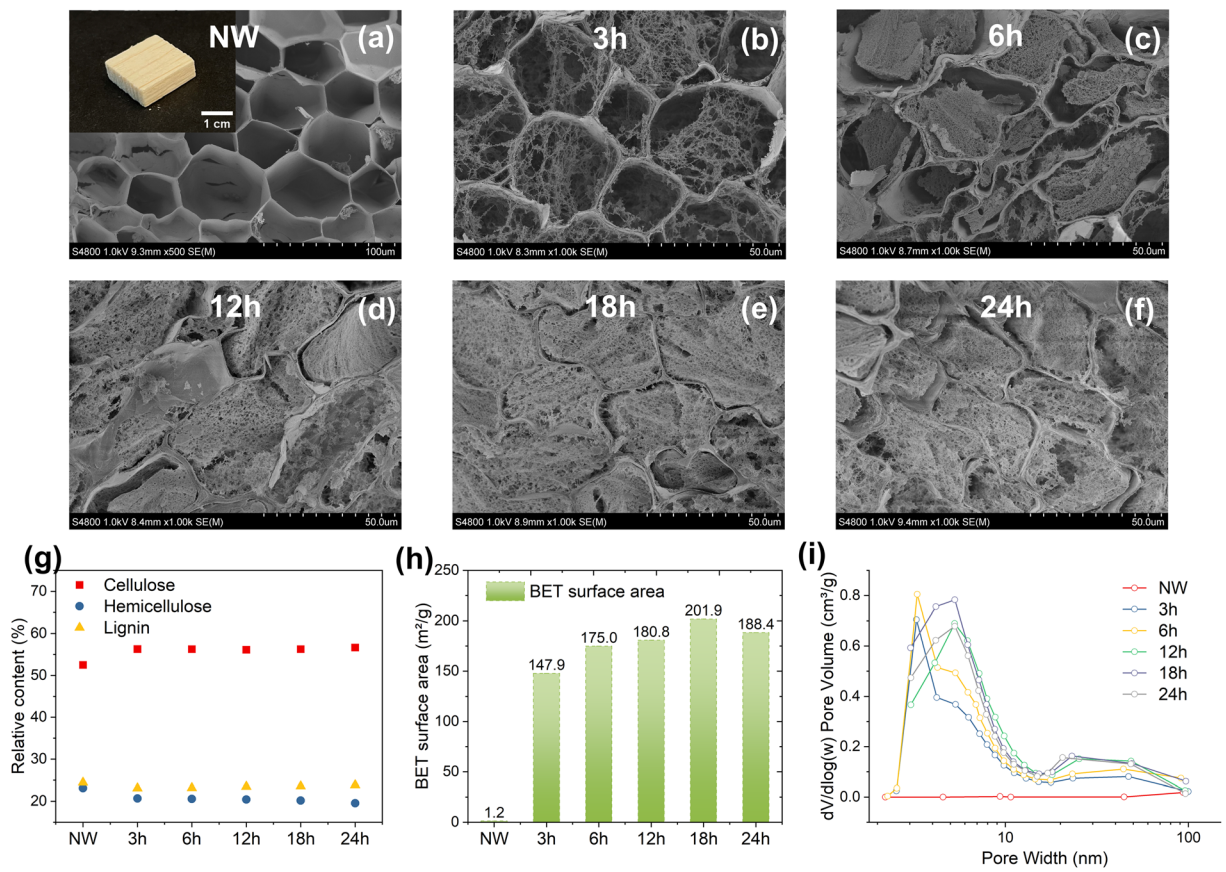

Fig. 2 (a) Photograph and SEM image of NW, (b)–(f) SEM images of wood samples *via* treatment time of 3 h, 6 h, 12 h, 18 h, 24 h, (g) relative content of cellulose, hemicellulose and lignin, (h) BET specific surface area and (i) pore size distribution of samples *via* different treatment time.

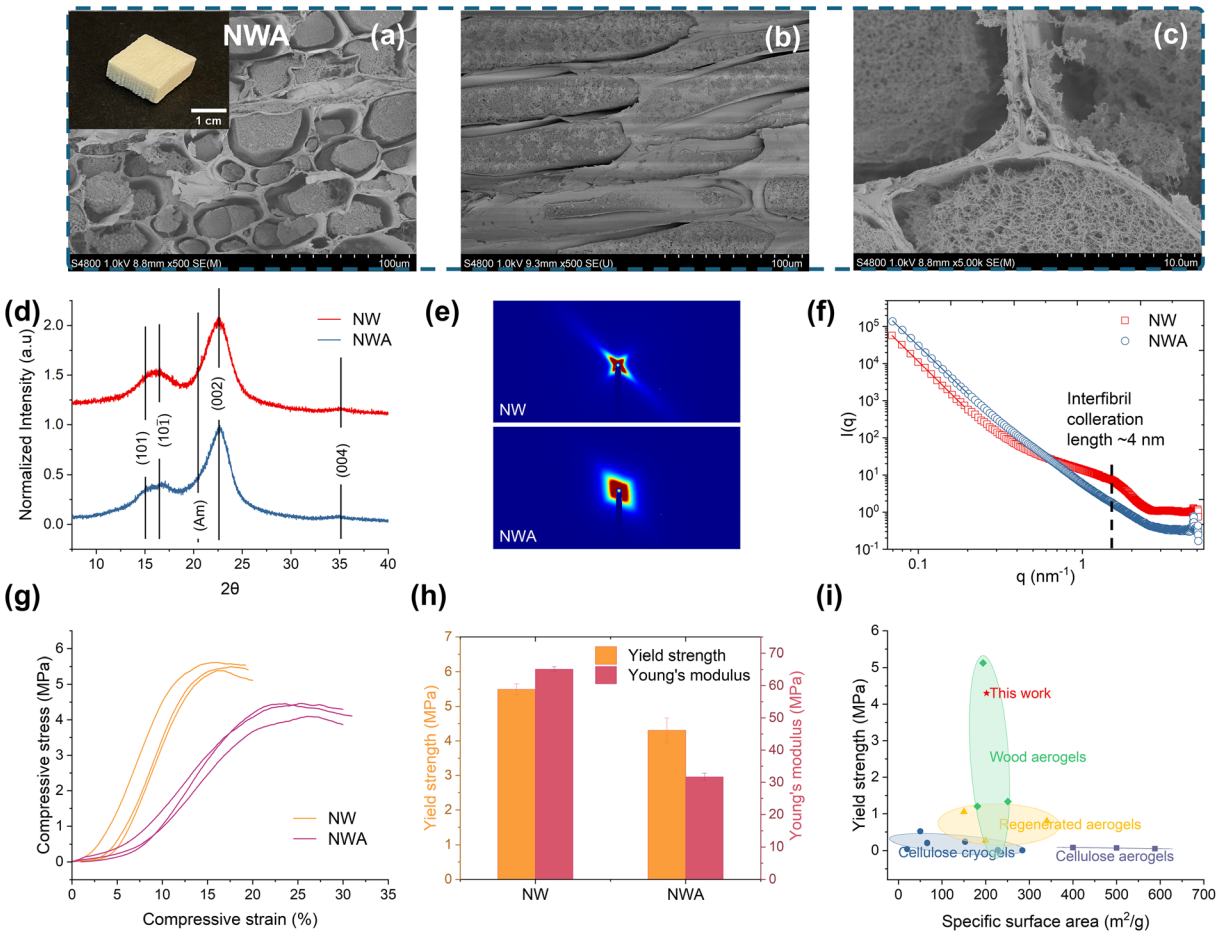

Fig. 3 (a) Photograph and SEM images of NWA from transverse plane, (b) tangential plane, and (c) cell wall corner. (d) XRD diffraction of NW and NWA. (e) 2D small-angle X-ray scattering patterns of NW and NWA, (f) corresponding 1D scattering line profiles. (g) strain–stress curves of NW and NWA along longitudinal direction, (h) compressive strength and Young's modulus of NW and NWA, (i) yield strength against SSA from cellulose cryogels,[45–49] cellulose aerogels,[50–52] regenerated aerocellulose,[53,54] reported wood aerogels[6,7,24] and NWA in this work.

are present between cell walls and fibril networks, possibly due to shrinkage of network phase during freeze-drying. The cross-sectional shape of cells changed from polygon (NW) to irregular shape (NWA), owing to the partial removal of cell wall components (especially in cell wall corners) and irregular cell wall swelling. The contour variation of the cell wall could also be observed from never-dried samples (Fig. S2). Cell wall swelling is reflected by the increased cell wall thickness. Double cell wall thickness of NWA increased to 0.8–1.2 μm, compared to that of NW (0.4–0.8 μm), as shown in Fig. 6b.

X-ray diffraction (XRD) was conducted to evaluate the cellulose type of wood templates, as shown in Fig. 3d. Both NW and NWA show distinct cellulose I peaks (101, 002, 040), implying the cellulose crystalline type remains the same after NaOH treatment. This is in line with the 10 wt% NaOH-treated poplar[38] and pine[39] for 90 minutes. Only a slight decrease in the degree of crystallinity was found in poplar wood.[38] Cellulose II was not observed on the XRD pattern of pine, despite the extended treatment time.[39] Small-angle X-ray scattering (SAXS) was applied to understand the nanostructure. Fig. 3e shows the 2D SAXS patterns. NW exhibits a strong narrow streak perpendicular to the fiber axis, owing to the preferable alignment of cellulose nanofibrils along the fiber axis. In comparison, NWA displays a diamond-shaped scattering with stronger isotropic components. The random distribution of network microfibrils decreased the overall anisotropy of NWA. The plot of scattering intensity $I(q)$ as a function of the scattering vector q (Fig. 3f) was extracted from the 2D SAXS patterns. The $I(q)$ curve of NW showed a broad shoulder centered at q = 1.58 nm^{-1}, corresponding to a length scale of 4 nm using Bragg's law ($d = 2\pi/q$).[40] This could be attributed to the correlation distance of oriented cellulose microfibrils in the cell walls.[40,41] The feature is no longer present in the NWA, indicating a less ordered structure, which could be explained by swelling of the cell wall and the rearrangement of cell wall biopolymers. In addition, NWA has higher intensity at low q range, indicating the presence of larger structures, corresponding to the generation of fibril networks. A slope $\approx q^{-4}$ was fitted at low q-values for both NW and NWA, which could be assigned to the surfaces of large pores and fiber lumina,[41–43]

in support of the preserved cellular structure after NaOH treatment.

Mechanical properties of NW and NWA were investigated through compression tests, as presented in Fig. 3g (longitudinal direction) and Fig. S3 (transversal direction). NWA shows larger strain at onset of compressive failure, and slightly lower strength (maximum stress) and modulus both in longitudinal and radial directions. A low stress region is present at the beginning, possibly due to sample surface roughness. After a linear region, maximum stress was observed at large strain. In the longitudinal direction, NWA possesses decreased compressive yield strength (σ_y = 4.3 MPa) and stiffness (E = 50 MPa) compared with NW (σ_y = 5.5 MPa, E = 65 MPa), as shown in Fig. 3h. Natural wood is known to fail by cell wall buckling in longitudinal compression.[44] Partial removal of hemicellulose may facilitate this mechanism by reducing cell wall properties. Fig. 3i compiles the compressive strength of cellulosic aerogels. NWA in this study has higher compressive strength than wood aerogels prepared by DMAc/LiCl[6] and [MTBD][MMP],[7] stemming from the preservation of lignin. Its strength is slightly lower than reported lignocellulosic wood aerogel[24] due to the lower density of our raw material. Nevertheless, the compressive strength of NWA still significantly outperforms cellulosic aerogels from bottom-up strategies,[45–54] owing to the oriented, tubular cellular structure of natural wood, as well as cellulose fibril alignment in the cell wall. In addition, the combination of high SSA and mechanical strength of NWA also stands out in Fig. 3i, since high SSA may facilitate functionalization so that applications of cellulosic aerogels can be extended.

The porous structure of wood aerogel is studied in detail to understand structure–property relationships. Fig. 4a shows the adsorption and desorption curves of NW and NWA. NW is a macroporous material, indicated by its isotherm type III plot. NWA displays the isotherm type IV, demonstrating its mesoporous structure. Pore size distribution from physisorption is shown in Fig. 4b. NW has a small volume of pores larger than 100 nm. By contrast, NWA shows a way larger pore volume, mainly including pores smaller than 10 nm (highlighted by a blue rectangle), and large pores ranging from 20–100 nm (highlighted by an orange rectangle). High-magnification SEM images of NWA (Fig. 4c and d) were acquired to assist the study of the porous structure. A great number of tiny pores were found in the cell wall (Fig. 4c), ascribing to the swelling of the cell wall and the loss of cell wall components (*e.g.*, hemicellulose). Pore size in the cell wall varies from 5–15 nm (Fig. 4e), contributing to the first peak (blue) of NWA in Fig. 4b. However, in the cell wall of NW, microfibril bundles are tightly packed with negligible appearance of pores (Fig. S4). In addition, the newly formed networks of NWA (Fig. 4d) contain pores from 15–95 nm (Fig. 4f), resulting in the second peak (orange in Fig. 4b). In other words, the mesoporous structure of wood aerogel measured by gas adsorption here consists of cell wall porosity and lumen network porosity, where cell wall porosity dominates the pore volume. The generation of mesopores significantly increases the SSA of NWA to 202 $m^2\ g^{-1}$, compared with that of NW (1.2 $m^2\ g^{-1}$).

The composition of lumen networks is important in deciphering aerogel structure. Fibril networks were isolated from wood aerogel for the first time and studied in detail, as demonstrated in Fig. 5a. Wet samples were cut into thin slices with thickness around 0.5 mm, aiming to create open pores. With the help of directional freezing, the network materials in

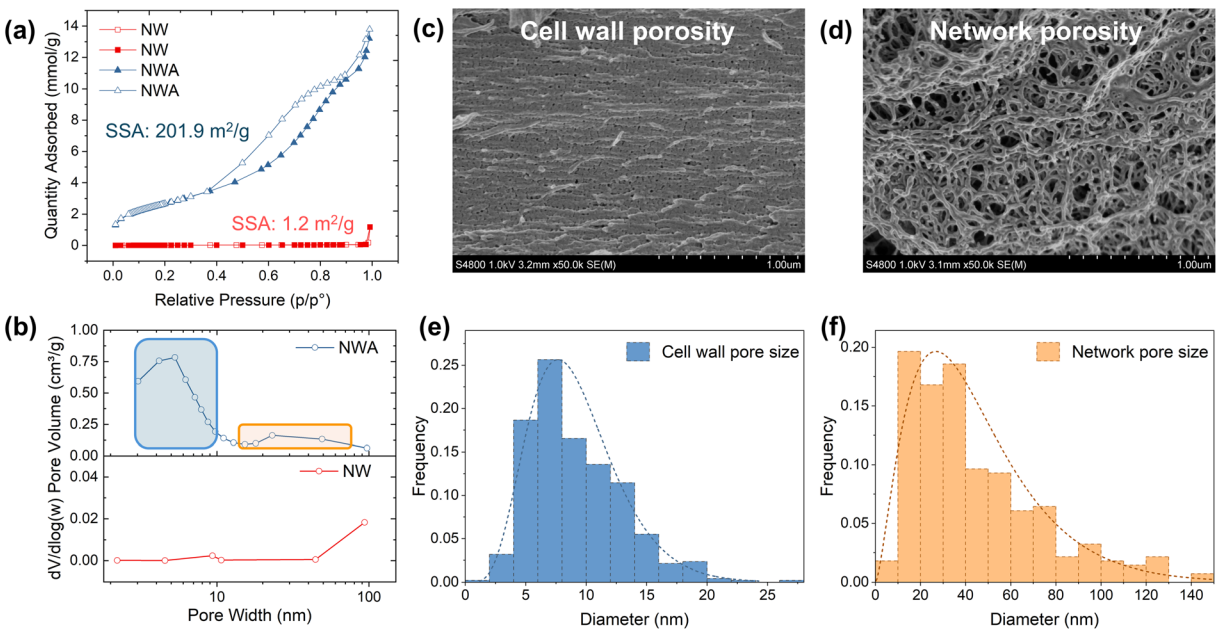

Fig. 4 Mesoporous structure characterization of wood aerogels. (a). Isotherm adsorption and desorption curves and BET specific surface area of NW and NWA, (b) pore size distribution of NW and NWA. SEM images showing (c) cell wall porosity and (d) network porosity in NWA, corresponding diameter histogram of pores (e) in the cell wall, and (f) among fibril networks.

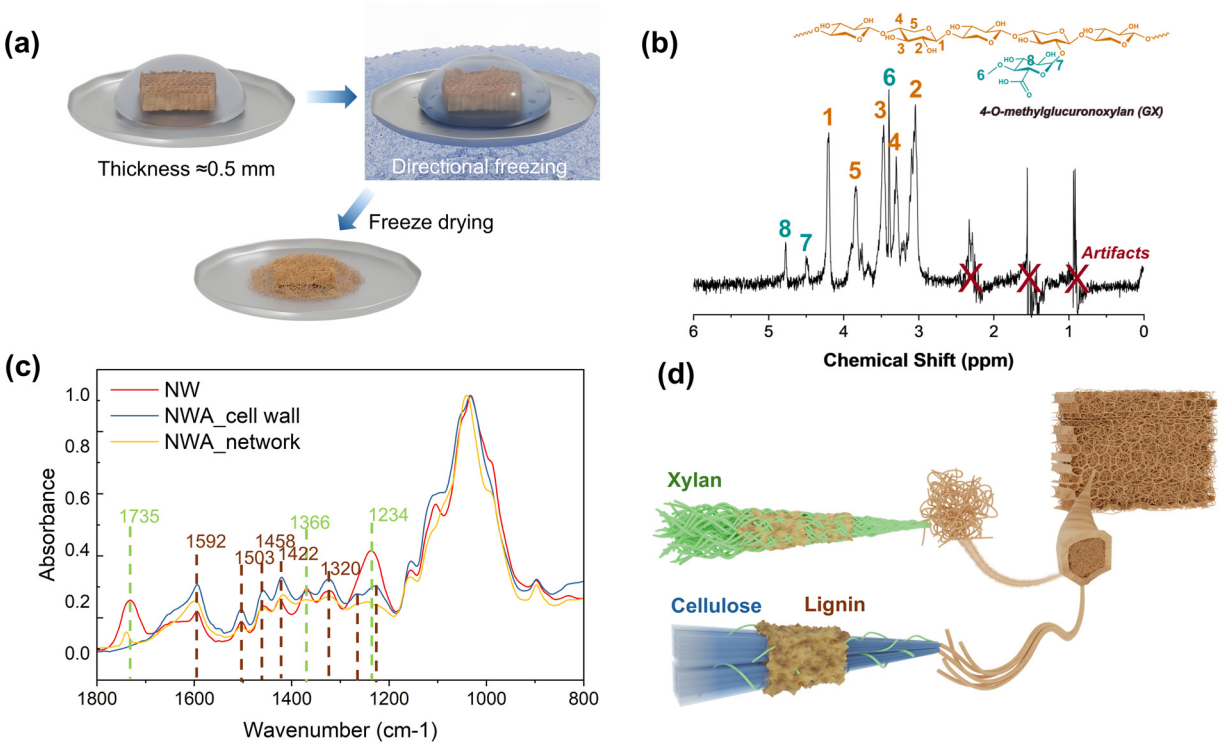

Fig. 5 (a) Schematic diagram of utilizing directional freezing to isolate fibril networks from NWA, (b) diffusion-edited ^{1}H NMR spectra of separated networks, (c) FTIR spectrum of NW, cell wall and networks of NWA, (d) schematic showing the composition of cell wall and network fibrils of NWA (blue crystals represent cellulose, green fibrils indicate xylan/hemicellulose and brown clusters represent lignin).

lumina were pushed out from thin slices due to the growth of ice. Sublimation of ice facilitated the formation of fibril-like materials (Fig. S5) on top and around wood slices, which were then collected for analysis and represented microfibril networks.

Isolated networks were dissolved in DMSO/[P_{4444}][OAc] (80 : 20) for diffusion-edited ^{1}H NMR experiments, following the protocol described by Fliri *et al.*,[55] in order to identify the composition of NWA fibril networks, as shown in Fig. 5b. Diffusion-edited ^{1}H NMR revealed the predominance of deacetylated glucuronoxylan (GX) in the extracted networks. Signal assignment here is in line with NW composition[56] and birch GX spectrum reported by Kilpeläinen *et al.*[57] No cellulose or acetyl groups were found through this analysis. 1D diffusion-ordered spectroscopy (DOSY) experiment (Fig. S6) further confirms the nature of the sample. Low diffusivity signals (3–4 × 10^{-11} m^2 s^{-1}) (corresponding to high molecular weight) are associated with the GX backbone repeating unit (xylose), while the low-intensity signal at higher diffusivity (3.5–5 × 10^{-10} m^2 s^{-1}) is related to the methylglucuronic acid substituent. In other words, newly formed networks seem to be mainly composed of polymeric xylan. Variation in xylan–cellulose interactions may explain this observation. Hardwood xylan backbone contains *O*-acetyl groups and 4-*O*-methylglucuronic acid, which are usually on even-numbered residues.[58] This specific substitution pattern could facilitate interactions with cellulose microfibrils in the plant cell wall.[59] If the substitution pattern is disrupted, the interaction between xylan and cellulose fibrils will be weakened.[60] During alkali treatment, acetyl functions are easily cleaved,[58] while 4-*O*-methylglucuronic acid substituent can be liberated in smaller quantities.[61] Acetyl cleavage can be observed by *in situ* diffusion-edited ^{1}H NMR analysis of the solute fraction, reproduced in 10 wt% NaOD (Fig. S7). Signals associated with acetyl functions (2.7–3.9 ppm, also around 2 ppm) emerged after 30 minutes and increased with reaction time. Minor presence of methylglucuronic acid on networks was also confirmed by DOSY (Fig. S6). Overall, the hydrolysis of acetyl functions and peeling of glucuronic acid substituents impair the specific decorations on xylan, weakening interactions between xylan and cellulose microfibrils. Consequently, the deacetylated xylan primarily contributes to the formation of networks in NWA.

FTIR was also carried out to identify the component variation during NaOH treatment (Fig. 5c). Due to the substantial density difference and corresponding peak intensity between networks and cell wall, the spectrum acquired from bulk NWA could be presumed to represent the cell wall of NWA. Peaks at 1366 cm^{-1} and 1230 cm^{-1} can be assigned to aliphatic C–H stretching in methyl carbohydrates and C–O stretching, respectively,[62,63] which are commonly used to indicate hemicellulose.[32,62,63] The intensity of these two peaks turns lower in both cell wall and network of NWA, consistent with

lower hemicellulose content in NWA (Fig. 2g). The peak at 1735 cm^{-1} is associated with C=O stretching and C=O vibrations in carbonyl,[64] commonly suggesting *O*-acetyl groups in xylan.[33] Interestingly, the characteristic peak of acetyl xylan in NW is no longer visible in the cell wall of NWA, while it turns smaller and sharper in the aerogel network. This variation indicates major xylan relocation from cell wall to network during NaOH treatment, consistent with diffusion-edited ^{1}H NMR (Fig. 5b) and DOSY results (Fig. S6). The blue-shifted small peak in the network at 1740 cm^{-1} might result from glucuronic acid substituents. Characteristic peaks of lignin,[65] 1592 cm^{-1}, 1505 cm^{-1}, 1458 cm^{-1}, 1425 cm^{-1}, and 1315 cm^{-1} appear in both cell wall and networks of NWA, indicating the presence of lignin in these structures. Their normalized intensity peaks increased in the cell wall of NWA, two small shoulder peaks at 1266 cm^{-1} and 1226 cm^{-1} can also be identified, which are related to the C–O of guaiacyl ring.[65] Lignin is more condensed upon NaOH treatment, the increase of phenolic groups was found due to the breaking of β-O-4 linkages,[11,66] which could explain the increased intensity of lignin-related peaks.

To summarize the information on NWA composition, the cell wall of NWA primarily consists of cellulose with minor hemicellulose content and lignin (Fig. 5c), while network fibrils are predominantly composed of deacetylated xylan (Fig. 5b), as displayed in Fig. 5d. Lignin is also likely present in the fibril network.

Mass diffusion from cell wall is critical for wood aerogel formation.[7] Therefore, the morphology change on the timescale was tracked to study the development of microfibril networks, as shown in Fig. 6. Once NW reacted with NaOH, the contour of cell walls deformed substantially (Fig. 6a). Distinct cell wall swelling was observed, as counted in Fig. 6b, average double cell wall thickness of treated wood doubled to 1.2 μm from 0.6 μm of NW. NaOH also causes partial liberation of cell wall materials (Fig. 6a). At the very beginning of diluting NaOH (Fig. 6c), detached materials were located close to the cell wall, and the lumen space still seemed to be empty. On the third day (Fig. 6d), the liberated substances (mainly deacetylated xylan) slightly moved away from the cell wall, reorientated, and intertwined, resulting in partially filled lumina. When NaOH was completely washed off (Fig. 6e), enough time was given for deacetylated xylan to rearrange and fully occupy the lumen space.

Overall, NaOH (10 wt%) at room temperature resulted in substantial cell wall swelling and cleavage of acetyl groups. Swollen cell walls and impaired specific substitutions on xylan liberated deacetylated xylan from the cell wall, thereby increasing cell wall porosity (Fig. 4c). Deacetylated xylan gradually diffused into and occupied the lumina, precipitated and reconstructed networks upon freeze-drying, contributing to network porosity (Fig. 4d).

The methodology developed for wood aerogel fabrication is universal and scalable. Different wood species (both hardwood and softwood) were tested using ambient temperature NaOH treatment, including birch, ash, and pine (Fig. 7a–d). Treatment time was extended to 24 h due to their higher densities compared with balsa. Newly formed network varies depending on the wood species. NaOH-treated birch displays

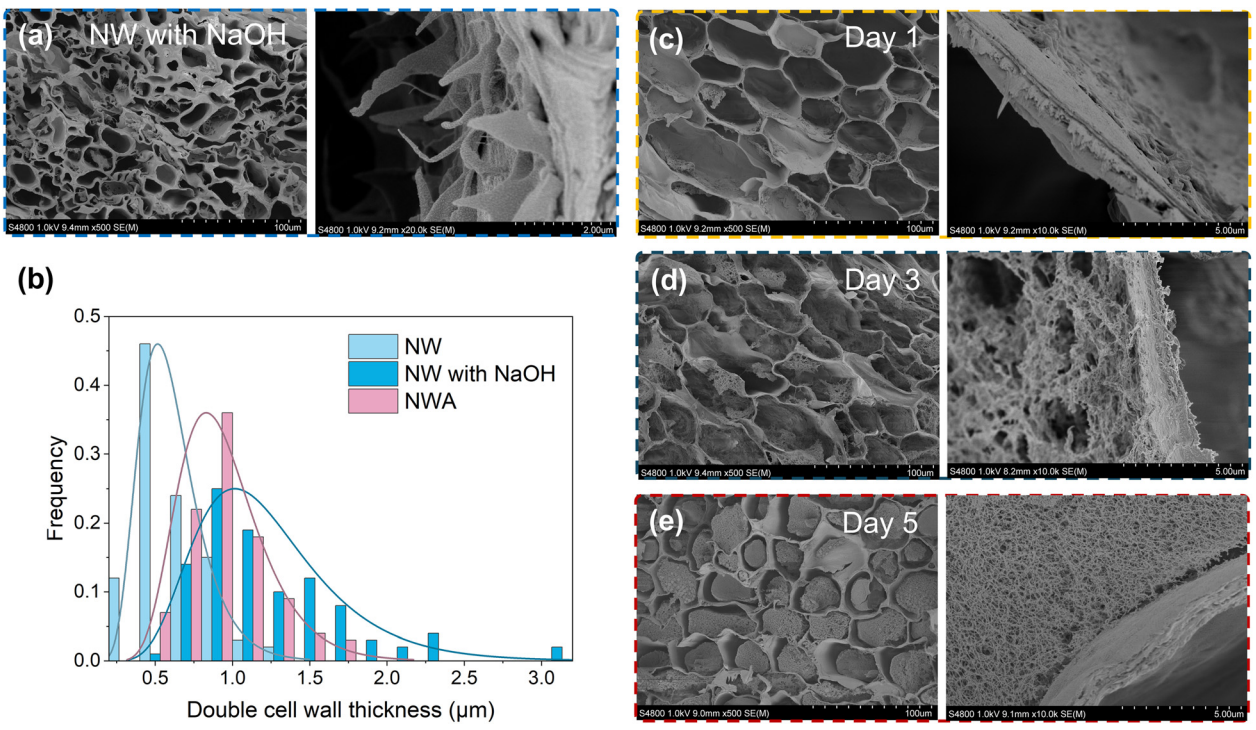

Fig. 6 (a) Cross-section and cell wall morphology of NW right after NaOH treatment, SEM images showing substance separated from the cell wall, (b) double cell wall thickness histogram of NW, NW with NaOH and NWA, (c)–(e) SEM images showing the morphology evolution during aerogel formation, including partial liberation of cell wall materials to gradual filling of lumen with fibril networks.

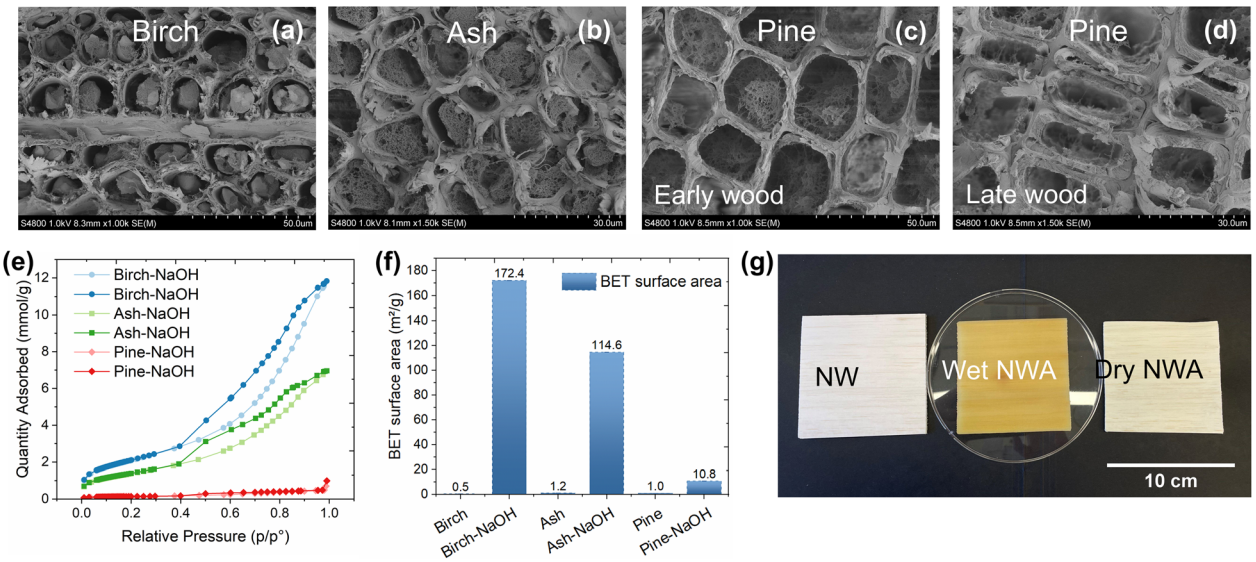

Fig. 7 Universality and scalability of the approach. SEM images on the cross-section of (a) NaOH-treated birch, (b) NaOH-treated ash, (c) NaOH-treated pine on early wood region and (d) late wood region. (e) isotherm adsorption and desorption curves, (f) BET surface of different wood species after 24 h NaOH treatment, (g) photography of wet and dry NWA at large scale.

dense networks in lumen (Fig. 7a). Less dense microfibril networks were observed for ash (Fig. 7b), because higher density of native ash (thicker cell walls) makes mass diffusion harder. NaOH-treated pine has sparse fibril networks in lumen in the early wood region (Fig. 7c), even less networks in the late wood (Fig. 7d), due to the difference in cell wall thickness and hemicellulose type. This suggests that diffusion kinetics plays an important role. Low density of wood with thinner cell walls facilitates the diffusion and therefore wood aerogel formation. Besides, NaOH treatment is more effective in hardwood than softwood for aerogel synthesis, due to its glucuronoxylan-rich hemicellulose.[67,68] Birch-NaOH and ash-NaOH display apparent isotherm type IV, as shown in Fig. 7e. SSA was significantly increased from approximately 1 m^2 g^{-1} for native wood to 172 m^2 g^{-1} for birch-NaOH and 115 m^2 g^{-1} for ash-NaOH (Fig. 7f). However, pine upon NaOH treatment only shows a small improvement in SSA (10.8 m^2 g^{-1}). The upscaling of the protocol was easily achieved, Fig. 7g shows large NWA samples with dimensions 8 × 8 × 0.5 cm^3.

The methodology developed here aligns with green engineering principles, from the choice of feedstock to the processing steps. The foundation of this approach is wood, a renewable resource that actively contributes to atmospheric CO_2 fixation (1.8 kg CO_2 per kg wood).[69,70] In addition, direct use of wood substrates presents a substantial energy advantage over strategies that rely on nanocellulose, as evidenced by high cumulative energy demand (CED) needed for nanocellulose fabrication: 9–14 MJ kg^{-1} for kraft pulp[71] and over 1000 MJ kg^{-1} for nanocellulose fabrication from pulp fiber (*e.g.*, homogenization requires 1050 MJ kg^{-1} while TEMPO oxidation requires 2420 MJ kg^{-1}).[72] The greenness of our aerogel processing is further highlighted by two factors. Ambient temperature treatment eliminates the need for electrical energy consumed in reported heating[24] or freezing[12] conditions for wood aerogel fabrication. The selection of NaOH, whose production entails a far lower energy (2.34–2.92 MJ kg^{-1} from bipolar membrane electrodialysis[73] and 4.97 MJ kg^{-1} from direct electrosynthesis[74]) than the organic solvents (>60 MJ kg^{-1})[75] used in other reported systems.[6,7] As a result, this work provides a green framework for wood aerogel synthesis towards advanced materials design.

Experimental

Materials and chemicals

Balsa wood (*Ochroma pyramidale*) of density 102 ± 5 kg m^{-3}, birch (*Betula pendula*, 476 ± 21 kg m^{-3}), ash (*Fraxinus excelsior*, 592 ± 43 kg m^{-3}), and pine (*Pinus*, 575 ± 39 kg m^{-3}) were bought from Material AB, Sweden. Samples of dimensions 15 × 15 × 5 mm^3 (longitudinal × tangential × radial) for balsa and 10 × 10 × 3 mm^3 for other species were cut for chemical treatment. Sodium hydroxide (NaOH, ≥98%), *tert*-butanol ($(CH_3)_3COH$, ≥99.0%) were bought from Sigma-Aldrich, Sweden, and ethanol absolute from VWR, Sweden.

Room temperature wood aerogel synthesis

Wood templates were introduced to a 10 wt% NaOH solution at the concentration of 1 wt% wood materials by weight. Wood soaked in NaOH was kept at room temperature for 3–24 h, and a vacuum was used to help the diffusion of NaOH. Subsequently, NaOH was washed off from wood templates with deionized water twice a day for a week until the supernatant was neutral in pH. Afterward, samples were exchanged

into a mixture of *tert*-butanol : H_2O (80 : 20) and then freeze-dried (−110 °C) at least 48 h for further characterization. *tert*-Butanol helped to reduce the size of ice crystals[76] and preserve the fibril network structure in the lumen.

Characterization

The morphology was observed in a field emission scanning electron microscopy (FE-SEM), Hitachi S-4800, Japan. Cross-sections of wood aerogels were prepared by freeze-fracture in liquid nitrogen (−196 °C), followed by freeze-drying. All samples were sputter-coated prior to analysis with a gold/palladium coating of ≈5 nm, using a Cressington 208HR, UK, for 30 s.

The specific surface area (SSA) was obtained by nitrogen physisorption using 3Flex Micromeritics. Samples were dried *via* Critical Point Drying (CPD) to prevent the collapse of pores due to capillary pressure gradient. Wood aerogels were gradually exchanged from water to ethanol. The mild supercritical condition of CO_2 (73.8 bar, 31.1 °C) greatly reduced the surface tension, keeping porous structure intact. Before physisorption, CPD-dried samples were degassed at 90 °C for 3000 minutes to remove the contamination and provide access to all surface area. Specimens were analyzed under the relative pressure 0.05–0.995P/P_0 in liquid nitrogen (−196 °C). SSA was determined between 0.05–0.25P/P_0 *via* the Brunauer–Emmett–Teller (BET) model,[77] while the Barret–Joyner–Halenda model gave information on pore size distribution from the desorption isotherm.

Functional groups were characterized using a Fourier transform infrared (FTIR), PerkinElmer Spectrum 100 FTIR spectrometer. The spectra were obtained over the range of 4000–600 cm^{-1}.

X-ray diffraction (XRD) was performed using a PANalytical X'Pert Pro powder diffractometer through Cu Kα radiation at 40 mA and 45 kV. The scans were performed over 2θ of 5–45° with a step size of 0.01° and scan speed of 0.02° s^{-1}.

Small-angle X-ray scattering (SAXS) measurements were conducted on a point collimated Anton Paar's SAXS point 2.0 system equipped with a microfocus X-ray source (Cu Kα radiation, wavelength 1.5418 Å, beam size of 500 μm). Eiger R 1 M horizontal detector (pixel size of 75 × 75 μm^2) was used for SAXS with the sample-to-detector distance of 575.7 mm. The exposure time of each measurement was 10 min and three frames were acquired. Before measurement, wood aerogels were cut into 5 × 15 × 5 mm^3 and mounted with the beam perpendicular to the fiber alignment. The data processing was performed by the SAXS analysis package (Anton Paar, Graz, Austria).

Lignin and carbohydrate content were obtained by first grinding the samples in a Wiley mill, followed by hydrolysis with 72% sulphuric acid at room temperature and 2.5% sulphuric acid in autoclave at 125 °C for 1 h. The hydrolyzed mixture was thereafter filtered to separate the lignin from carbohydrates. Lignin content was quantified using the standard method: TAPPI T 222 om-2. The filtered solution was diluted for carbohydrate analysis *via* Dionex ICS-300 ion chromatography (Thermo Fisher Scientific Inc.).

Compression properties were evaluated *via* Instron 5944 with a 500 N load cell at a rate of 10% strain per min. Samples with approximate dimensions of 5 × 7.5 × 7.5 mm^3 (longitudinal × tangential × radial) were used for longitudinal compression, while dimensions of 15 × 15 × 5 mm^3 for radial compression. Mechanical tests were performed at 50% relative humidity and 23 °C. All samples were conditioned for at least 3 days prior to measurements. Compression strength was acquired through the stress at the yield point, where the structure collapsed. The yield point was determined at the intersection of the tangents from the initial elastic region and subsequent plateau. Young's moduli were calculated from the slope of the linear elastic region in the stress–strain curves.

Liquid-state diffusion-edited ^1H NMR was used to check the composition of aerogel networks and *in situ* analysis of the solute fraction. NWA network samples (1 wt%) were dissolved in DMSO-d_6 : [P4444][OAc] (80 : 20 w/w) at 65 °C following the protocol described in the literature.[55] In addition, to investigate the wood components dissolved during NaOH treatment, the protocol was reproduced with deuterated solvent. Sodium hydride was used to prepare *in situ* 10 wt% NaOD in D_2O. Solute aliquots were collected during NaOD treatment from 30 min to 24 h. Measurements were made using a Bruker Avance III HD 400 MHz. The diffusion-edited 1H experiment used a 1D diffusion-ordered spectroscopy (DOSY) pulse sequence based on stimulated echo and bipolar gradient pulses (Bruker pulse program 'ledbpgp2s1d'), with 3 s relaxation delay ($d1$), 0.5 s acquisition time (aq), 16 dummy scans (ds), 512 transient scans (ns), a sweep-width (sw) of 20 ppm with the transmitter offset on 6.1 ppm (o1p), diffusion time ($d20$) of 200 ms, gradient recovery delay ($d16$) of 0.2 ms, eddy current delay ($d21$) of 5 ms, diffusion gradient pulse duration ($p30$) of 2.5 ms, and z-gradient strength (gpz6) of 80% at >50 G cm^{-1} (probe z-gradient strength). Acquisitions were performed at 338 K. Data were processed with MestreNova (Mestrelab Research) software using a 90° shifted square sine-bell apodization window, baseline and phase correction were applied.

Conclusions

Highly mesoporous wood aerogels with a SSA of 202 m^2 g^{-1} and a yield strength of 4.3 MPa were prepared using 10 wt% NaOH treatment at ambient temperature. Different from conventional cellulose dissolution and regeneration, ambient temperature NaOH swelled the cell wall and impaired the specific substitutions on xylan. Deacetylated xylan migrated out from cell walls and reconstructed the networks in lumina. High SSA derives from both cell wall pores (*via* swelling and biopolymer extraction) and lumen fibril networks. The high mechanical strength is ascribed to the preserved cellular alignment of wood. This study elucidates the role of NaOH in bulk wood modification and reveals new possibilities for cell wall engineering. The developed methodology for wood aerogel fab-

rication is green and scalable, with the potential to treat other cellulosic materials (*e.g.*, bamboo) or hemicellulose-rich agricultural residues (*e.g.*, corn cobs and wheat straw). Additionally, the obtained aerogel structure could serve as a versatile porous platform for advanced functionalization.

Author contributions

The manuscript was written through contributions of all authors. All authors have given approval to the final version of the manuscript. All the authors provided critical feedback and edited the manuscript. Xiaoying Xu: methodology, data curation, formal analysis, investigation, visualization, writing – original draft, writing – reviewing & editing. Arezu Sehati: methodology, data curation, writing – reviewing & editing. Lukas Marcos Celada: investigation, data curation, writing – reviewing & editing. Peter Olsén: writing – reviewing & editing. Lars Berglund: funding acquisition, writing – reviewing & editing. Yuanyuan Li: supervision, funding acquisition, writing – reviewing & editing.

Conflicts of interest

The authors declare no competing financial interest.

Data availability

The data supporting this article have been included as part of the supplementary information (SI). Supplementary information is available. See DOI: https://doi.org/10.1039/d5gc03785a.

Acknowledgements

The authors are very grateful for the support from Wallenberg Wood Science Center (WWSC 2.0: KAW 2018.0452), KAW 2021.0311, and FORMAS (2023-01695). Zha L.'s help with carbohydrate analysis is highly appreciated. We are thankful for the support from Treesearch infrastructure and RISE for SAXS measurements. Zhao W. and Yu S. are thanked for sharing their knowledge on X-ray scattering.

References

1 T. Budtova, Cellulose II Aerogels: A Review, *Cellulose*, 2019, **26**(1), 81–121, DOI: 10.1007/s10570-018-2189-1.
2 P. Gupta, B. Singh, A. K. Agrawal and P. K. Maji, Low Density and High Strength Nanofibrillated Cellulose Aerogel for Thermal Insulation Application, *Mater. Des.*, 2018, **158**, 224–236, DOI: 10.1016/j.matdes.2018.08.031.
3 M. Dilamian and B. Noroozi, Rice Straw Agri-waste for Water Pollutant Adsorption: Relevant Mesoporous Super Hydrophobic Cellulose Aerogel, *Carbohydr. Polym.*, 2021, **251**, 117016, DOI: 10.1016/j.carbpol.2020.117016.
4 H. Sai, R. Fu, L. Xing, J. Xiang, Z. Li, F. Li and T. Zhang, Surface Modification of Bacterial Cellulose Aerogels' Web-like Skeleton for Oil/Water Separation, *ACS Appl. Mater. Interfaces*, 2015, **7**(13), 7373–7381, DOI: 10.1021/acsami.5b00846.
5 D. A. Osorio, B. E. J. Lee, J. M. Kwiecien, X. Wang, I. Shahid, A. L. Hurley, E. D. Cranston and K. Grandfield, Cross-Linked Cellulose Nanocrystal Aerogels As Viable Bone Tissue Scaffolds, *Acta Biomater.*, 2019, **87**, 152–165, DOI: 10.1016/j.actbio.2019.01.049.
6 J. Garemark, X. Yang, X. Sheng, O. Cheung, L. Sun, L. A. Berglund and Y. Li, Top-Down Approach Making Anisotropic Cellulose Aerogels as Universal Substrates for Multifunctionalization, *ACS Nano*, 2020, **14**(6), 7111–7120, DOI: 10.1021/acsnano.0c01888.
7 J. Garemark, J. E. Perea-Buceta, D. Rico del Cerro, S. Hall, B. Berke, I. Kilpeläinen, L. A. Berglund and Y. Li, Nanostructurally Controllable Strong Wood Aerogel toward Efficient Thermal Insulation, *ACS Appl. Mater. Interfaces*, 2022, **14**(21), 24697–24707, DOI: 10.1021/acsami.2c04584.
8 H. Sun, H. Bi, X. Lin, L. Cai and M. Xu, Lightweight, Anisotropic, Compressible, and Thermally-Insulating Wood Aerogels with Aligned Cellulose Fibers, *Polymers*, 2020, **12**(1), 165.
9 W. He, J. Cao, F. Guo, Z. Guo, P. Zhou, R. Wang, S. Liang, Q. Pang, B. Wei, Y. Jiao, *et al.*, Nanostructured Carboxylated-Wood Aerogel Membrane for High-Efficiency Removal of Cu(II), Ions from Wastewater, *Chem. Eng. J.*, 2023, **468**, 143747, DOI: 10.1016/j.cej.2023.143747.
10 W. Zhang, C. Xu, X. Che, T. Wang, S. Willför, M. Li and C. Li, Encapsulating Amidoximated Nanofibrous Aerogels within Wood Cell Tracheids for Efficient Cascading Adsorption of Uranium Ions, *ACS Nano*, 2022, **16**(8), 13144–13151, DOI: 10.1021/acsnano.2c06173.
11 J. Garemark, F. Ram, L. Liu, I. Sapouna, M. F. Cortes Ruiz, P. T. Larsson and Y. Li, Advancing Hydrovoltaic Energy Harvesting from Wood through Cell Wall Nanoengineering, *Adv. Funct. Mater.*, 2023, **33**(4), 2208933, DOI: 10.1002/adfm.202208933.
12 Y. Li, J. Cui, H. Shen, C. Liu, P. Wu, Z. Qian, Y. Duan and D. Liu, Useful Spontaneous Hygroelectricity from Ambient Air by Ionic Wood, *Nano Energy*, 2022, **96**, 107065, DOI: 10.1016/j.nanoen.2022.107065.
13 S. Wang, L. Li, L. Zha, S. Koskela, L. A. Berglund and Q. Zhou, Wood Xerogel for Fabrication of High-performance Transparent Wood, *Nat. Commun.*, 2023, **14**(1), 2827, DOI: 10.1038/s41467-023-38481-x.
14 Z. Zhu, S. Fu and L. A. Lucia, A Fiber-Aligned Thermal-Managed Wood-Based Superhydrophobic Aerogel for Efficient Oil Recovery, *ACS Sustainable Chem. Eng.*, 2019, **7**(19), 16428–16439, DOI: 10.1021/acssuschemeng.9b03544.
15 W. He, H. Qiang, S. Liang, F. Guo, R. Wang, J. Cao, Z. Guo, Q. Pang, B. Wei and J. Sun, Hierarchically Porous Wood Aerogel/polypyrrole(PPy) Composite Thick Electrode for

Supercapacitor, *Chem. Eng. J.*, 2022, **446**, 137331, DOI: 10.1016/j.cej.2022.137331.

16 Q. Zhang, L. Li, B. Jiang, H. Zhang, N. He, S. Yang, D. Tang and Y. Song, Flexible and Mildew-Resistant Wood-Derived Aerogel for Stable and Efficient Solar Desalination, *ACS Appl. Mater. Interfaces*, 2020, **12**(25), 28179–28187, DOI: 10.1021/acsami.0c05806.

17 J. Song, C. Chen, Z. Yang, Y. Kuang, T. Li, Y. Li, H. Huang, I. Kierzewski, B. Liu, S. He, *et al.*, Highly Compressible, Anisotropic Aerogel with Aligned Cellulose Nanofibers, *ACS Nano*, 2018, **12**(1), 140–147, DOI: 10.1021/acsnano.7b04246.

18 W. Kong, C. Wang, C. Jia, Y. Kuang, G. Pastel, C. Chen, G. Chen, S. He, H. Huang, J. Zhang, *et al.*, Muscle-Inspired Highly Anisotropic, Strong, Ion-Conductive Hydrogels, *Adv. Mater.*, 2018, **30**(39), 1801934, DOI: 10.1002/adma.201801934.

19 G. Chen, T. Li, C. Chen, W. Kong, M. Jiao, B. Jiang, Q. Xia, Z. Liang, Y. Liu, S. He, *et al.*, Scalable Wood Hydrogel Membrane with Nanoscale Channels, *ACS Nano*, 2021, **15**(7), 11244–11252, DOI: 10.1021/acsnano.0c10117.

20 J. Zhang, Z. Hu, Y. Hou, C. Wu and W. Ding, Wood Hydrogel for Efficient Moisture-Electric Generation, *ACS Appl. Polym. Mater.*, 2024, **6**(15), 8856–8865, DOI: 10.1021/acsapm.4c00959.

21 K. Nie, Z. Wang, R. Tang, L. Zheng, C. Li, X. Shen and Q. Sun, Anisotropic, Flexible Wood Hydrogels and Wrinkled, Electrodeposited Film Electrodes for Highly Sensitive, Wide-Range Pressure Sensing, *ACS Appl. Mater. Interfaces*, 2020, **12**(38), 43024–43031, DOI: 10.1021/acsami.0c13962.

22 S. Wang, H. Chen, K. Li, S. Koskela, L. A. Berglund and Q. Zhou, Strong, Transparent, and Thermochromic Composite Hydrogel from Wood Derived Highly Mesoporous Cellulose Network and PNIPAM, *Composites, Part A*, 2022, **154**, 106757, DOI: 10.1016/j.compositesa.2021.106757.

23 S. Wang, K. Li and Q. Zhou, High Strength and Low Swelling Composite Hydrogels from Gelatin and Delignified Wood, *Sci. Rep.*, 2020, **10**(1), 17842, DOI: 10.1038/s41598-020-74860-w.

24 J. Garemark, J. E. Perea-Buceta, M. Felhofer, B. Chen, M. F. Cortes Ruiz, I. Sapouna, N. Gierlinger, I. A. Kilpeläinen, L. A. Berglund and Y. Li, Strong, Shape-Memory Lignocellulosic Aerogel via Wood Cell Wall Nanoscale Reassembly, *ACS Nano*, 2023, **17**(5), 4775–4789, DOI: 10.1021/acsnano.2c11220.

25 N. Mosier, C. Wyman, B. Dale, R. Elander, Y. Y. Lee, M. Holtzapple and M. Ladisch, Features of Promising Technologies for Pretreatment of Lignocellulosic Biomass, *Bioresour. Technol.*, 2005, **96**(6), 673–686, DOI: 10.1016/j.biortech.2004.06.025.

26 H. Sobue, H. Kiessig and K. Hess, *The Cellulose-Sodium Hydroxide-Water System As a Function of the Temperature*; 1990.

27 T. Budtova and P. Navard, Cellulose in NaOH–water Based Solvents: A Review, *Cellulose*, 2016, **23**(1), 5–55, DOI: 10.1007/s10570-015-0779-8.

28 A. Ishikawa, T. Okano and J. Sugiyama, Fine Structure and Tensile Properties of Ramie Fibres in the Crystalline Form of Cellulose I, II, IIII and IVI, *Polymer*, 1997, **38**(2), 463–468, DOI: 10.1016/S0032-3861(96)00516-2.

29 R. M. Rowell, *Handbook of Wood Chemistry and Wood Composites*, CRC Press, 2005. DOI: 10.1201/b12487.

30 U. Henniges, M. Kostic, A. Borgards, T. Rosenau and A. Potthast, Dissolution Behavior of Different Celluloses, *Biomacromolecules*, 2011, **12**(4), 871–879, DOI: 10.1021/bm101555q.

31 M. E. Himmel, S.-Y. Ding, D. K. Johnson, W. S. Adney, M. R. Nimlos, J. W. Brady and T. D. Foust, Biomass Recalcitrance: Engineering Plants and Enzymes for Biofuels Production, *Science*, 2007, **315**(5813), 804–807, DOI: 10.1126/science.1137016.

32 R. Sun, J. M. Lawther and W. B. Banks, Fractional and Structural Characterization of Wheat Straw Hemicelluloses, *Carbohydr. Polym.*, 1996, **29**(4), 325–331, DOI: 10.1016/S0144-8617(96)00018-5.

33 W. Farhat, R. Venditti, A. Quick, M. Taha, N. Mignard, F. Becquart and A. Ayoub, Hemicellulose Extraction and Characterization for Applications in Paper Coatings and Adhesives, *Ind. Crops Prod.*, 2017, **107**, 370–377, DOI: 10.1016/j.indcrop.2017.05.055.

34 R. C. Sun, J. M. Fang, J. Tomkinson, Z. C. Geng and J. C. Liu, Fractional Isolation, Physico-Chemical Characterization and Homogeneous Esterification of Hemicelluloses from Fast-Growing Poplar Wood, *Carbohydr. Polym.*, 2001, **44**(1), 29–39, DOI: 10.1016/S0144-8617(00)00196-X.

35 T. Okano and A. Sarko, Mercerization of Cellulose I. X-ray Diffraction Evidence for Intermediate Structures, *J. Appl. Polym. Sci.*, 1984, **29**(12), 4175–4182, DOI: 10.1002/app.1984.070291247.

36 T. Okano and A. Sarko, Mercerization of Cellulose. II., Alkali–Cellulose Intermediates and a Possible Mercerization Mechanism, *J. Appl. Polym. Sci.*, 1985, **30**(1), 325–332, DOI: 10.1002/app.1985.070300128.

37 W. Geng, R. Narron, X. Jiang, J. J. Pawlak, H.-m. Chang, S. Park, H. Jameel and R. A. Venditti, The Influence of Lignin Content and Structure on Hemicellulose Alkaline Extraction for Non-Wood and Hardwood Lignocellulosic Biomass, *Cellulose*, 2019, **26**(5), 3219–3230, DOI: 10.1007/s10570-019-02261-y.

38 B. Doczekalska and M. Zborowska, Wood Chemical Composition of Selected Fast Growing Species Treated with NaOH. Part I: Structural Substances, *Wood Res.*, 2010, **55**, 41–48.

39 S. Borysiak and B. Doczekalska, X-ray Diffraction Study of Pine Wood Treated with NaOH, *Fibres Text. East. Eur.*, 2005, **13**(5), 87–89.

40 P. Chen, Y. Li, Y. Nishiyama, S. V. Pingali, H. M. O'Neill, Q. Zhang and L. A. Berglund, Small Angle Neutron Scattering Shows Nanoscale PMMA Distribution in Transparent Wood Biocomposites, *Nano Lett.*, 2021, **21**(7), 2883–2890, DOI: 10.1021/acs.nanolett.0c05038.

41 H. F. Jakob, S. E. Tschegg and P. Fratzl, Hydration Dependence of the Wood-Cell Wall Structure in Picea abies. A Small-Angle X-ray Scattering Study, *Macromolecules*, 1996, **29**(26), 8435–8440, DOI: 10.1021/ma9605661.

42 H. F. Jakob, D. Fengel, S. E. Tschegg and P. Fratzl, The Elementary Cellulose Fibril in Picea abies: Comparison of Transmission Electron Microscopy, Small-Angle X-ray Scattering, and Wide-Angle X-ray Scattering Results, *Macromolecules*, 1995, **28**(26), 8782–8787, DOI: 10.1021/ma00130a010.

43 Y. Nishiyama, P. Langan, H. O'Neill, S. V. Pingali and S. Harton, Structural Coarsening of Aspen Wood by Hydrothermal Pretreatment Monitored by Small- and Wide-Angle Scattering of X-rays and Neutrons on Oriented Specimens, *Cellulose*, 2014, **21**(2), 1015–1024, DOI: 10.1007/s10570-013-0069-2.

44 L. J. Gibson and M. F. Ashby, *Cellular Solids: Structure and Properties*; Cambridge University Press, 1997. DOI: 10.1017/CBO9781139878326.

45 M. Pääkkö, J. Vapaavuori, R. Silvennoinen, H. Kosonen, M. Ankerfors, T. Lindström, L. A. Berglund and O. Ikkala, Long and Entangled Native Cellulose I Nanofibers Allow Flexible Aerogels and Hierarchically Porous Templates for Functionalities, *Soft Matter*, 2008, **4**(12), 2492–2499, DOI: 10.1039/B810371B.

46 H. Sehaqui, M. Salajková, Q. Zhou and L. A. Berglund, Mechanical Performance Tailoring of Tough Ultra-High Porosity Foams Prepared from Cellulose I Nanofiber Suspensions, *Soft Matter*, 2010, **6**(8), 1824–1832, DOI: 10.1039/B927505C.

47 H. Sehaqui, Q. Zhou and L. A. Berglund, High-Porosity Aerogels of High Specific Surface Area Prepared from Nanofibrillated Cellulose (NFC), *Compos. Sci. Technol.*, 2011, **71**(13), 1593–1599, DOI: 10.1016/j.compscitech.2011.07.003.

48 S. Xiao, R. Gao, Y. Lu, J. Li and Q. Sun, Fabrication and Characterization of Nanofibrillated Cellulose and Its Aerogels from Natural Pine Needles, *Carbohydr. Polym.*, 2015, **119**, 202–209, DOI: 10.1016/j.carbpol.2014.11.041.

49 F. Jiang and Y.-L. Hsieh, Cellulose Nanofibril Aerogels: Synergistic Improvement of Hydrophobicity, Strength, and Thermal Stability via Cross-Linking with Diisocyanate, *ACS Appl. Mater. Interfaces*, 2017, **9**(3), 2825–2834, DOI: 10.1021/acsami.6b13577.

50 Y. Kobayashi, T. Saito and A. Isogai, Aerogels with 3D Ordered Nanofiber Skeletons of Liquid-Crystalline Nanocellulose Derivatives as Tough and Transparent Insulators, *Angew. Chem., Int. Ed.*, 2014, **53**(39), 10394–10397, DOI: 10.1002/anie.201405123.

51 S. F. Plappert, J.-M. Nedelec, H. Rennhofer, H. C. Lichtenegger and F. W. Liebner, Strain Hardening and Pore Size Harmonization by Uniaxial Densification: A Facile Approach toward Superinsulating Aerogels from Nematic Nanofibrillated 2,3-Dicarboxyl Cellulose, *Chem. Mater.*, 2017, **29**(16), 6630–6641, DOI: 10.1021/acs.chemmater.7b00787.

52 D. Sivaraman, G. Siqueira, A. K. Maurya, S. Zhao, M. M. Koebel, G. Nyström, M. Lattuada and W. J. Malfait, Superinsulating Nanocellulose Aerogels: Effect of Density and Nanofiber Alignment, *Carbohydr. Polym.*, 2022, **292**, 119675, DOI: 10.1016/j.carbpol.2022.119675.

53 M. Schestakow, I. Karadagli and L. Ratke, Cellulose Aerogels Prepared from an Aqueous Zinc Chloride Salt Hydrate Melt, *Carbohydr. Polym.*, 2016, **137**, 642–649, DOI: 10.1016/j.carbpol.2015.10.097.

54 R. Sescousse, R. Gavillon and T. Budtova, Aerocellulose from Cellulose–Ionic Liquid Solutions: Preparation, Properties and Comparison with Cellulose–NaOH and Cellulose–NMMO Routes, *Carbohydr. Polym.*, 2011, **83**(4), 1766–1774, DOI: 10.1016/j.carbpol.2010.10.043.

55 L. Fliri, K. Heise, T. Koso, A. R. Todorov, D. R. del Cerro, S. Hietala, J. Fiskari, I. Kilpeläinen, M. Hummel and A. W. T. King, Solution-State Nuclear Magnetic Resonance Spectroscopy of Crystalline Cellulosic Materials Using a Direct Dissolution Ionic Liquid Electrolyte, *Nat. Protoc.*, 2023, **18**(7), 2084–2123, DOI: 10.1038/s41596-023-00832-9.

56 M. Borrega, P. Ahvenainen, R. Serimaa and L. Gibson, Composition and Structure of Balsa (Ochroma Pyramidale) Wood, *Wood Sci. Technol.*, 2015, **49**(2), 403–420, DOI: 10.1007/s00226-015-0700-5.

57 A. W. T. King, V. Mäkelä, S. A. Kedzior, T. Laaksonen, G. J. Partl, S. Heikkinen, H. Koskela, H. A. Heikkinen, A. J. Holding, E. D. Cranston, I. Kilpeläinen, *et al.*, Liquid-State NMR Analysis of Nanocelluloses, *Biomacromolecules*, 2018, **19**(7), 2708–2720, DOI: 10.1021/acs.biomac.8b00295.

58 E. Sjöström, Chapter 3 - WOOD POLYSACCHARIDES, in *Wood Chemistry*, ed. E. Sjöström, Academic Press, 2nd edn, 1993, pp. 51–70.

59 M. Busse-Wicher, T. C. F. Gomes, T. Tryfona, N. Nikolovski, K. Stott, N. J. Grantham, D. N. Bolam, M. S. Skaf and P. Dupree, The Pattern of Xylan Acetylation Suggests Xylan May Interact with Cellulose Microfibrils As a Twofold Helical Screw in the Secondary Plant Cell Wall of Arabidopsis Thaliana, *Plant J.*, 2014, **79**(3), 492–506, DOI: 10.1111/tpj.12575.

60 N. J. Grantham, J. Wurman-Rodrich, O. M. Terrett, J. J. Lyczakowski, K. Stott, D. Iuga, T. J. Simmons, M. Durand-Tardif, S. P. Brown, R. Dupree, *et al.*, An Even Pattern of Xylan Substitution Is Critical for Interaction with Cellulose In Plant Cell Walls, *Nat. Plants*, 2017, **3**(11), 859–865, DOI: 10.1038/s41477-017-0030-8.

61 M. H. Johansson and O. Samuelson, Reducing End Groups In Birch Xylan and Their Alkaline Degradation, *Wood Sci. Technol.*, 1977, **11**(4), 251–263, DOI: 10.1007/BF00356924.

62 J. Sun, H. Guo, J. Ribera, C. Wu, K. Tu, M. Binelli, G. Panzarasa, F. W. M. R. Schwarze, Z. L. Wang and I. Burgert, Sustainable and Biodegradable Wood Sponge Piezoelectric Nanogenerator for Sensing and Energy Harvesting Applications, *ACS Nano*, 2020, **14**(11), 14665–14674, DOI: 10.1021/acsnano.0c05493.

63 M. Poletto, A. J. Zattera and R. M. C. Santana, Structural Differences Between Wood Species: Evidence from Chemical Composition, FTIR Spectroscopy, and Thermogravimetric Analysis, *J. Appl. Polym. Sci.*, 2012, **126**(S1), E337–E344, DOI: 10.1002/app.36991.

64 J. Lehto, J. Louhelainen, T. Kłosińska, M. Drożdżek and R. Alén, Characterization of Alkali-Extracted Wood by FTIR-ATR Spectroscopy, *Biomass Convers. Biorefin.*, 2018, **8**(4), 847–855, DOI: 10.1007/s13399-018-0327-5.

65 K. K. Pandey, A Study of Chemical Structure of Soft and Hardwood and Wood Polymers by FTIR Spectroscopy, *J. Appl. Polym. Sci.*, 1999, **71**(12), 1969–1975, DOI: 10.1002/(SICI)1097-4628(19990321)71:12<1969::AID-APP6>3.0.CO;2-D.

66 D.-y. Min, H.-m. Chang, H. Jameel, L. Lucia, Z.-g. Wang and Y.-c. Jin, The Structure of Lignin of Corn Stover and Its Changes Induced by Mild Sodium Hydroxide Treatment, *BioResources*, 2014, **9**(2), 2405–2414.

67 M. S. Bay, K. Karimi, M. Nasr Esfahany and R. Kumar, Structural Modification of Pine and Poplar Wood by Alkali Pretreatment to Improve Ethanol Production, *Ind. Crops Prod.*, 2020, **152**, 112506, DOI: 10.1016/j.indcrop.2020.112506.

68 R. C. Pettersen, The Chemical Composition of Wood, in *The Chemistry of Solid Wood, Advances in Chemistry*, American Chemical Society, 1984, vol. 207, pp. 57–126.

69 R. D. Bergman, M. Puettmann, A. Taylor and K. E. Skog, The Carbon Impacts of Wood Products, *For. Prod. J.*, 2014, **64**(7–8), 220–231, DOI: 10.13073/fpj-d-14-00047.

70 N. Zeng, Carbon sequestration via wood burial, *Carbon Balance Manage.*, 2008, **3**(1), 1, DOI: 10.1186/1750-0680-3-1.

71 E. Oliaei, T. Lindström and L. A. Berglund, Sustainable Development of Hot-Pressed All-Lignocellulose Composites—Comparing Wood Fibers and Nanofibers, *Polymers*, 2021, **13**(16), 2747.

72 Q. Li, S. McGinnis, C. Sydnor, A. Wong and S. Renneckar, Nanocellulose Life Cycle Assessment, *ACS Sustainable Chem. Eng.*, 2013, **1**(8), 919–928, DOI: 10.1021/sc4000225.

73 G. P. Thiel, A. Kumar, A. Gómez-González and J. H. V. Lienhard, Utilization of Desalination Brine for Sodium Hydroxide Production: Technologies, Engineering Principles, Recovery Limits, and Future Directions, *ACS Sustainable Chem. Eng.*, 2017, **5**(12), 11147–11162, DOI: 10.1021/acssuschemeng.7b02276.

74 A. Kumar, F. Du and J. H. V. Lienhard, Caustic Soda Production, Energy Efficiency, and Electrolyzers, *ACS Energy Lett.*, 2021, **6**(10), 3563–3566, DOI: 10.1021/acsenergylett.1c01827.

75 S. Hellweg, U. Fischer, M. Scheringer and K. Hungerbühler, Environmental assessment of chemicals: methods and application to a case study of organic solvents, *Green Chem.*, 2004, **6**(8), 418–427, DOI: 10.1039/B402807B.

76 K. Yoshida, T. Yamaguchi, A. Kovalenko and F. Hirata, Structure of tert-Butyl Alcohol–Water Mixtures Studied by the RISM Theory, *J. Phys. Chem. B*, 2002, **106**(19), 5042–5049, DOI: 10.1021/jp013400x.

77 S. Brunauer, P. H. Emmett and E. Teller, Adsorption of Gases in Multimolecular Layers, *J. Am. Chem. Soc.*, 1938, **60**(2), 309–319, DOI: 10.1021/ja01269a023.